Article

Not peer-reviewed version

Balancing Transparency and Ferroelectricity in $K_{0.5}Na_{0.5}NbO_3$ Lead-Free Composite Ceramics

Lechen Dong , Xujun Li , Zhonghua Dai * , Yuanyuan Zheng , Chenxi Liu , Xin Zhao , Shuitao Gu

Posted Date: 12 September 2025

doi: 10.20944/preprints202509.1110.v1

Keywords: Relaxor ferroelectrics; Optical transmittance; Dielectric energy storage; Electro-optical functional devices

 doi:10.20944/preprints202509.1110.v1

Article

Balancing Transparency and Ferroelectricity in $K_{0.5}Na_{0.5}NbO_3$ Lead-Free Composite Ceramics

Lechen Dong [1], Xujun Li [1], Zhonghua Dai [2,*], Yuanyuan Zheng [1], Chenxi Liu [1], Xin Zhao [1] and Shuitao Gu [2,*]

[1] Shaanxi Province Key Laboratory of Thin Films Technology & Optical Test, School of Opto-electronic Engineering, Xi'an Technological University, Xi'an 710032, China

[2] School of Civil Engineering, Chongqing University, Chongqing 400044, China

* Correspondence: zhdai_xjtu@163.com (Z.D.); gust@cqu.edu.cn (S.G.)

Abstract

Transparent ferroelectric ceramics have garnered significant research interest in recent years owing to their unique optical transparency and electrical properties. Among them, potassium sodium niobate (KNN)-based ceramics stand out as a prominent lead-free ferroelectrics, exhibiting exceptional optoelectrical coupling performance due to their high Curie temperature, excellent ferroelectric properties, environmental friendliness, and optical transparency. In this work, an effective strategy involving multi-component doping in KNN-based materials is proposed. An energy density of 3.18 J/cm^3 along with a high efficiency of 79%, and a light transmittance of 71% at 1800 nm, are achieved in $K_{0.5}Na_{0.5}NbO_3$ lead-free composite ceramic, which exhibits fast discharging characteristics, with $t_{0.9}$ = 1.27 μs at the current density (C_D = 248.73 A/cm^2) and power density (P_D = 23.88 MW/cm^3). The strategy provides a feasible routine for combining energy storage functionality with optical transparency, illustrating its great potential to be generally applicable in the design of lead-free composite ceramics with excellent overall performance.

Keywords: Relaxor ferroelectrics; Optical transmittance; Dielectric energy storage; Electro-optical functional devices

1. Introduction

In recent years, lead-free transparent ferroelectric ceramics have emerged as promising multifunctional materials for advanced optoelectronic and energy storage applications, owing to their unique combination of optical transparency, ferroelectric behavior, and superior dielectric properties. While traditional lead-based ferroelectrics such as Pb(Zr,Ti)O3 have historically dominated this field due to their outstanding electromechanical performance, growing environmental concerns about their toxicity have driven the search for sustainable alternatives. Among these alternatives, potassium sodium niobate (KNN)-based ceramics have garnered significant attention as a representative ferroelectric material, exhibiting excellent ferroelectric characteristics, high Curie temperatures, and achievable optical transparency when properly engineered [1-3].

Achieving high optical transparency in ferroelectric ceramics requires precise control of several critical factors including near-theoretical density to minimize porosity, submicron-scale grain size below 1 μm to reduce light scattering, complete elimination of secondary phases, and isotropic crystal structure. Recent studies have demonstrated that strategic approaches such as rare-earth ion doping and solid solution formation can effectively modulate the bandgap while simultaneously suppressing birefringence and inducing polar nanoregions (PNRs), which play a pivotal role in optimizing energy storage performance through their unique field-responsive behavio r[4]. When subjected to an applied electric field, these PNRs enable rapid dipole alignment to generate substantial polarization, yet upon field removal spontaneously revert to a short-range disordered state characterized by

 doi:10.20944/preprints202509.1110.v1

minimal coercive field (E_c) and remnant polarization (P_r). This reversible polarization switching mechanism not only produces extremely small coercive fields and residual polarization but also significantly enhances overall energy storage performance by combining high efficiency with power density. The dynamic response of PNRs under electric fields thus provides an effective pathway to simultaneously improve both optical and electrical properties in ferroelectric ceramics [5-8].

Theoretically, the energy storage performance of ferroelectric materials is primarily determined by their polarization-electric field (P-E) loop characteristics. To achieve both high recoverable energy storage density (W_{rec}) and energy efficiency (η), three critical parameters must be simultaneously optimized: maximizing the saturation polarization (P_{max}), minimizing the remnant polarization (P_r), and significantly enhancing the breakdown strength (BDS) [9]. Over the past decade, substantial research efforts have focused on balancing these competing parameters to improve energy storage performance. Yang et al. achieved the W_{rec} of 2 J/cm^3 in 0.9$K_{0.5}Na_{0.5}NbO_3$-0.1$BiFeO_3$ (0.9KNN-0.1BF) ceramics at 206 kV/cm, which is superior to other lead-free dielectric ceramics under moderate electric fields (<220 kV/cm) [10]. Xing et al. investigated the energy storage properties of KNN-0.015EB ceramics with an energy storage density of W = 2.68 J/cm^3 and a recoverable energy storage density of W_{rec} = 1.85 J/cm^3 with good thermal stability [11].These examples still leave much to be desired in terms of transparency, and KNN ceramics have great potential as multifunctional materials for optical and energy storage applications, but significant challenges remain in balancing their transparency and ferroelectricity.

Enhancing breakdown strength remains the most effective approach for improving energy storage density, requiring comprehensive optimization of material composition, grain size reduction, grain boundary resistance improvement, density maximization, and defect minimization. Furthermore, careful tuning of phase structure and sintering processes can significantly improve material microstructure, thereby increasing both breakdown strength and dielectric reliability [12-14]. However, significant challenges persist in simultaneously optimizing optical transmittance, energy storage density, and efficiency in KNN-based systems. While grain refinement improves transparency and breakdown strength, excessive doping may degrade ferroelectric properties. Moreover, the complex relationships between microstructure, phase composition, and optoelectronic coupling mechanisms in these materials are not yet fully understood. Consequently, systematic investigation of microstructure-property relationships, optoelectronic coupling mechanisms, and performance optimization strategies in KNN transparent ferroelectric ceramics is crucial for advancing their practical applications in energy storage systems [15-18].

This study employs a multi-component doping strategy to simultaneously modulate both phase structure and microstructure, targeting synergistic enhancement of optical and energy storage properties in KNN-based ceramics. The co-doping of K^+/Bi^{3+} and Zn^{2+}/Nb^{5+} into the KNN lattice facilitates the formation and growth of polar nanoregions (PNRs) while reducing the average grain size to submicron scale, ultimately resulting in decreased residual polarization (P_r) and enhanced breakdown field strength (BDS). The 0.87(($K_{0.5}Na_{0.5}$)NbO_3)-0.13(($K_{0.296}Bi_{0.9}$)($Zn_{0.667}Nb_{0.334}$)O_3 ceramic exhibits outstanding performance with an optical transmittance (T%) of 71% at 1800 nm, an energy storage density (W) of 3.18 J/cm^3 at 220 KV/cm, a recoverable energy storage density (W_{rec}) of 2.51 J/cm^3, an energy storage efficiency (η) of 79%. These enhancements significantly improve the applicability of KNN-based transparent ferroelectric ceramics for contemporary energy storage applications, while the synergistic coupling between optical and electrical properties proves crucial for facilitating their integration into advanced optoelectronic systems.

2. Materials and Methods

The (1-x)(($K_{0.5}Na_{0.5}$)NbO_3)-x(($K_{0.296}Bi_{0.9}$)($Zn_{0.667}Nb_{0.334}$)O_3(KNN-KBZN) ceramics with compositions x = 0.08, 0.13, 0.18, and 0.23 were prepared through the solid-state method. High-purity precursor powders including K_2CO_3(99.9%), Na_2CO_3(99.9%), Nb_2O_5(99.5%), Bi_2O_3(999%) and ZnO (99%) were pre-dried at 80 °C for 24h, then ball-milled in ethanol for 24h. After calcination at 850 °C for 4h, the powders were pressed into pellets (10mm×2mm) with PVA binder at 20MPa and sintered

 doi:10.20944/preprints202509.1110.v1

at 1100-1150 °C for 4h in Al_2O_3 powder bed to prevent volatilization. The ceramics were then characterized for structural and functional properties.

XRD analysis was conducted using a diffractometer (40 kV, 15 mA) with 2θ scanning from 20° to 75° at 0.02° steps. Microstructure was examined by SEM (Hitachi SU1510, 15 kV). Dielectric properties were measured using an impedance analyzer (Agilent E4980A) with 1 °C temperature resolution. The optical transmittance (300-1200 nm) was measured using a Shimadzu UV-950 spectrophotometer. Ferroelectric *P-E* loops were measured using a Radiant Premier II system, while energy storage performance was evaluated with a LY20-10015 charge-discharge tester. *P-E* loop measurements were conducted using a ferroelectric tester (Premier II, Radiant Technologies, USA), while charge/discharge characteristics were evaluated with a dedicated testing system (LY20-10015).

3. Results and Discussion

Figure 1(a) shows the XRD patterns of KNN-KBZN ceramics in the 2θ range of 20° - 70°. All diffraction peaks correspond exclusively to a perovskite structure, confirming the formation of phase-pure materials without detectable secondary phases or impurity peaks. The results showed that the additive KBZN had fully diffused into the KNN lattice and formed a stable solid solution. Generally, the KNN-based ceramics can be characterized by quantitative analysis of the relative strengths of the (200) peaks in the range of 44° - 47°. In the absence of KBZN doping in the system, pure KNN ceramics were found to exhibit an orthorhombic phase with spontaneous polarization in the (101) direction. However, the transition from orthorhombic to tetragonal and from tetragonal to cubic can occur with an increase in KBZN doping, and the pseudo-cubic phase exhibits a single (200) diffraction peak in XRD pattern [19-21].

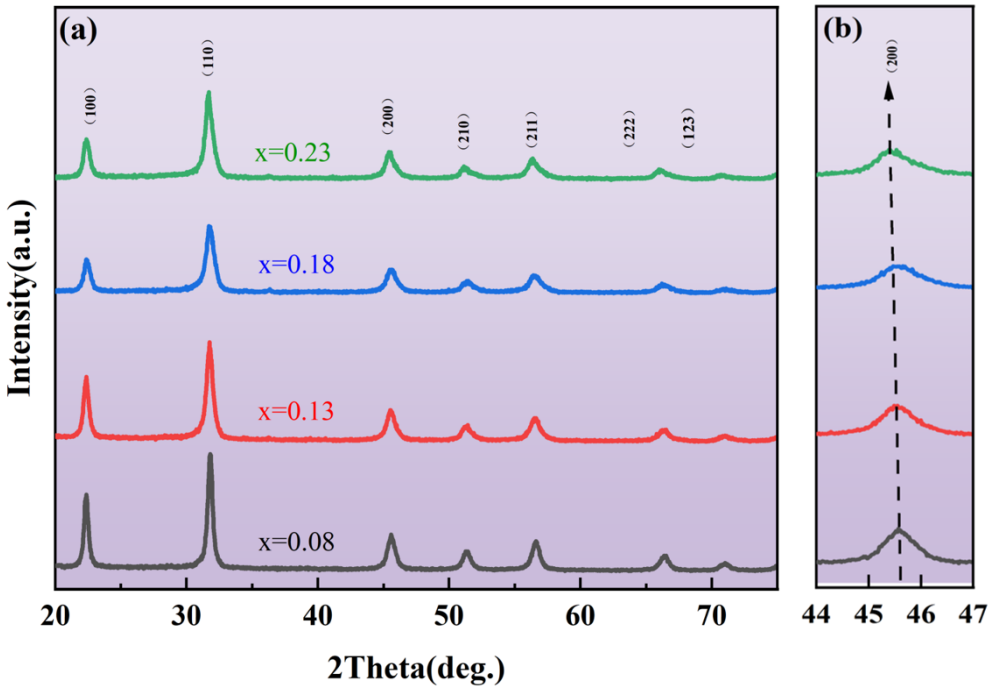

Figure 1. XRD patterns of (1-x)KNN-xKBZN (x=0.08, 0.13, 0.18, 0.23).

Figure 1(b) illustrates an enlarged view of Figure 1(a) from 44° - 47°. Only one (200) peak, observed near 45°, indicated that the sample exhibited a pseudocubic phase. It has been observed that crystals exhibiting a pseudocubic phase are isotropic. Consequently, the isotropic nature of these crystals results in minimal scattering at grain boundaries, thereby reducing the loss of light energy. Furthermore, as the concentration of KBZN increases, the (200) peak shifts to a lower angle, indicating an increase in cell volume. The introduction of dopant ions with mixed valence states and varying

 doi:10.20944/preprints202509.1110.v1

ionic radii significantly enhances structural disorder within the system, promoting both the formation of abundant polar nanoregions (PNRs) and substantial suppression of long-range ferroelectric ordering. These combined effects create favorable conditions for pseudocubic phase stabilization [22].

Figure 2(a)-(d) show the natural surface micromorphology of the ceramics after the addition of different contents of KBZN observed using scanning electron microscopy at room temperature. From the diagram, it can be seen that the introduction of KBZN significantly decreases the grain size of KNN (4-5 μm) ferroelectric ceramics (pure KNN) [23]. It is beneficial to improve the breakdown field strength of ceramic samples. Generally, grain growth depends on the migration of grain boundaries, and voids are the most important factors. Based on this, Gaussian fitting was performed using Nano-Scale software to obtain the particle size distribution curves for each composition. As shown in the figure, the average particle size of each composition is below 1 μm, ranging between 0.3 - 0.4 μm. The average particle size is 0.321 μm at $x = 0.13$. The results demonstrate that KBZN effectively suppresses ceramic grain growth, and smaller particle diameters correlate with higher breakdown field strength [24-26].

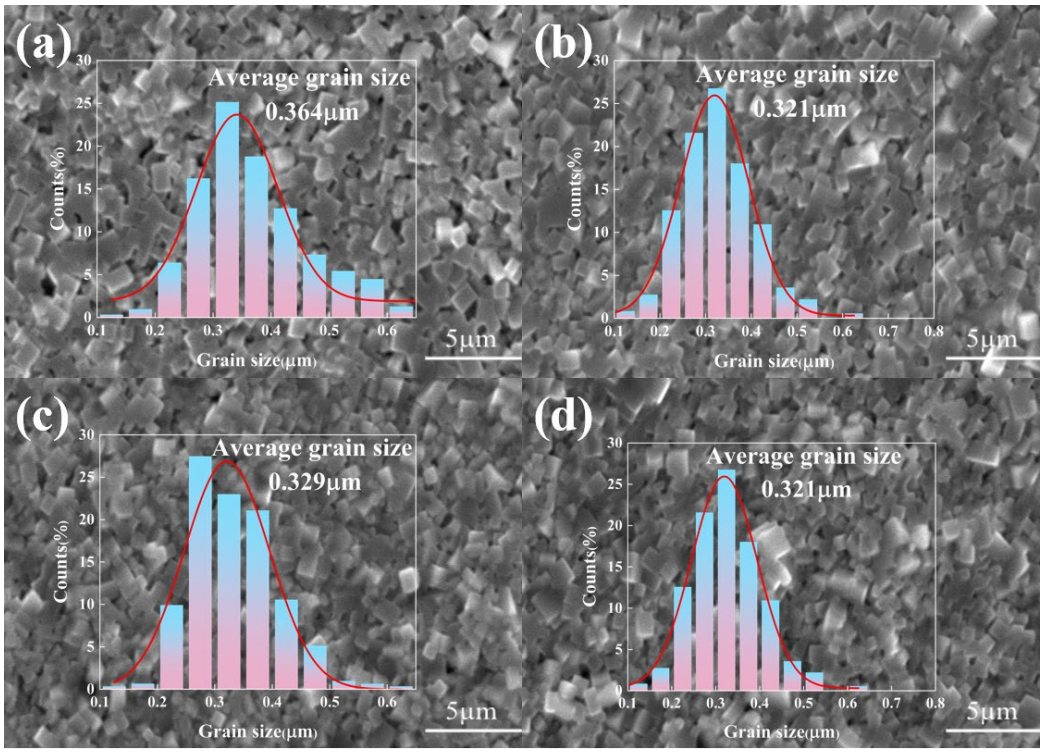

Figure 2. Surface SEM images of (1-x)KNN-xKBZN ceramics (x=0.08, 0.13, 0.18, 0.23).

Figure 3 shows the variation of dielectric constant and dielectric loss of (1-x)KNN-xKBZN lead-free relaxation ferroelectric ceramic samples as a function of temperature (-150-400°C) from 1KHz to 1000KHz. The results of dielectric characterization show that the relative dielectric constant values of all the compositions are about 1000, while there is a monotonically decreasing trend in the dielectric constant with the increase in the content of the KBZN di-phase, as shown in Figure 3. The dielectric loss is also in the lower range, the dielectric loss is smaller than 0.5, and all of them have remarkable relaxation properties. The dielectric maximum corresponds to the Curie temperature (T_c), marking the ferroelectric-paraelectric phase transition where the spontaneous polarization vanishes due to the transformation from dipolar order to disorder within ferroelectric domains. This transition is accompanied by a sequential structural evolution from orthorhombic to tetragonal and finally to cubic symmetry, as documented in reference [27-30].

 doi:10.20944/preprints202509.1110.v1

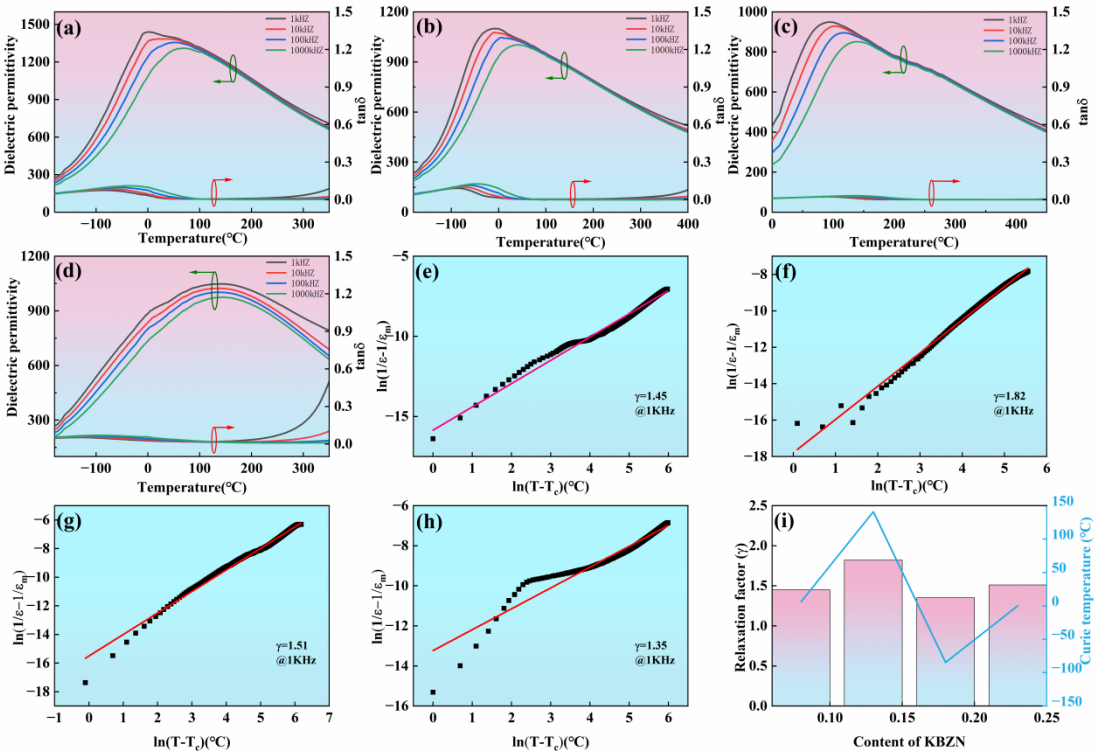

Figure 3. a-d) Dielectric temperature spectra; (e-i) fitted relaxation factor plots of (1-x)KNN-xKBZN ceramics (x=0.08, 0.13, 0.18, 0.23).

As illustrated in Figure 3(a)-(d), the Curie temperature (T_c) initially decreases and then steadily rises with increasing KBZN content, eventually shifting toward higher temperatures. The phase transition occurs over a broad temperature range, with individual components transitioning at distinct points, demonstrating pronounced diffuse phase transition behavior. Near T_c, the dielectric constant decreases at higher frequencies, accompanied by significant frequency dispersion—a hallmark of relaxor ferroelectrics. These observations confirm that the (1-x)KNN-xKBZN ($0.08<x<0.23$) system belongs to the relaxor ferroelectric family [31]. To further quantify its relaxor characteristics, the modified Curie-Weiss law was applied. The degree of material relaxation can be assessed using the relaxation factor, γ, which typically ranges from 1 to 2. When γ approaches 1, the material displays conventional ferroelectric behavior, whereas a value closer to 2 indicates relaxor ferroelectric properties. The γ value is determined by the following formula[32]:

$$\frac{1}{\varepsilon'} - \frac{1}{\varepsilon_m'} = \frac{(T - T_c)^{\gamma}}{C} \tag{1}$$

$$\gamma = \ln\left(\frac{1}{\varepsilon'} - \frac{1}{\varepsilon_m'}\right) / \ln(T - T_c) \tag{2}$$

In the equation, C represents the Curie constant, ε'_m denotes the peak dielectric constant at a specific frequency, T_c signifies the Curie temperature, and γ is the relaxation factor. The dielectric constant curves obtained at 1 kHz were linearly fitted, as shown in Figure 3(e)-(h), where the fitted curves for the relaxation factor at different doping concentrations are presented. From the plots, it is evident that the relaxation factors (γ) all exceed 1.3, confirming that the incorporation of the secondary component KBZN enhances the relaxor behavior of the KNN. The relaxation factor initially increases and then decreases with rising KBZN content, peaking at $\gamma = 1.82$ when $x = 0.13$[33,34].

 doi:10.20944/preprints202509.1110.v1

The energy storage density and energy storage efficiency of (1-x)KNN-xKBZN relaxation ferroelectric ceramics can be calculated by the following equations[35]:

$$W_{rec} = \int_{P_r}^{P_{max}} EdP \tag{3}$$

$$\eta = \frac{W_{rec}}{W_{rec} + W_{loss}} \tag{4}$$

Figure 4(a) displays the unipolar polarization-electric field (P-E) loops of (1-x)KNN-xKBZN ceramics at 150 kV/cm. Figure 4(b) shows the polarization characteristics at 150 kV/cm, which indicates that the maximum polarization (P_{max}) of (1-x)KNN-xKBZN ceramics increases and then decreases as the KBZN doping concentration is increased from 0.08 to 0.23, up to 27.48 μC/cm², and the residual polarization (P_r) values of all the samples remain below 5 μC/cm². Figure 4(c) depicts the unipolar polarization-electric field (P-E) loops of (1-x)KNN-xKBZN ceramics under the maximum applied different electric field (E_b). The P-E loops of each sample exhibit a "narrow" shape, attributed to the introduction of KBZN, which results in the disruption of the long-range ordered ferroelectric domains within the KNN matrix, replaced by short-range disordered polar nanoregions(PNRs). The formation of these PNRs not only reduces the P_r, but also significantly enhances the energy storage efficiency. The effective energy storage densities and energy storage efficiency of ceramics are presented in Figure 4(d), where the highest energy storage density is 3.18 J/cm³. With the increase of KBZN content, the effective energy storage density increases and then decreases, and the energy storage efficiency reaches 79% at x = 0.13, with the highest effective energy storage density of 2.51 J/cm³. Figure 4(e) presents the recoverable energy storage density and energy storage efficiency of 0.13KNN-0.87KBZN ceramic under different electric fields; The results reveal that W_{rec} increases monotonically with applied electric field, reaching a maximum value of 2.51 J/cm³ at 220KV/cm. As shown in Figure 4(f), Polarization of 0.13KNN-0.87KBZN ceramic under different electric fields. P_{max} demonstrates an initial linear increase with applied field, followed by a sublinear growth regime, ultimately reaching 34.15 μC/cm² at maximum field strength. P_r similarly shows field-dependent variation, though with different characteristic behavior. The energy storage performance of these ceramic materials is governed by multiple interrelated factors, including breakdown field strength, energy storage efficiency, and polarization capability. Rather than optimizing any single parameter in isolation, this study focused on achieving an optimal balance between these competing factors to maximize overall energy storage performance [36-39].

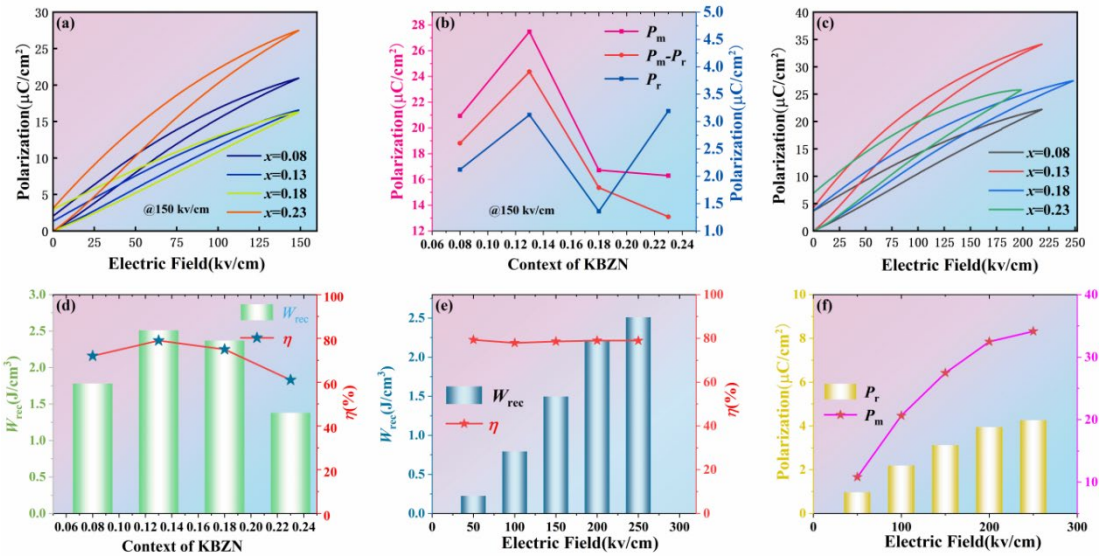

 doi:10.20944/preprints202509.1110.v1

Figure 4. a) P-E loops of (1-x)KNN-xKBZN ceramics at 150 kV/cm; (b) Polarization; (c) P-E loops at breakdown field strengths (d) recoverable energy storage density and energy storage efficiency; (e) recoverable energy storage density and energy storage efficiency of 0.87KNN-0.13KBZN ceramic under different electric fields; (f) Polarization of 0.87KNN-0.13KBZN ceramic under different electric fields.

To evaluate the practical application capability of the ceramics, the charge/discharge performance of the 0.87KNN-0.13KBZN ceramic was tested. Figure 5(a) shows the discharge curves under underdamped conditions (R=260 Ω), and Figure 5(c) shows the discharge curves under overdamped conditions (R=10000 Ω). Figure 5(b) clearly demonstrates that both current density (C_D) and power density (P_D) of the samples increase with applied electric field, achieving peak values of 248.73 A/cm² and 23.89 MW/cm³ respectively at 200 kV/cm. The field-dependent discharge characteristics presented in Figure 5(d) reveal that the discharge energy density shows a similar increasing trend with electric field. Notably, at 200 kV/cm, the system achieves a discharge time ($t_{0.9}$) of 1.27 μs, indicating ultrafast energy release capability [40,41]

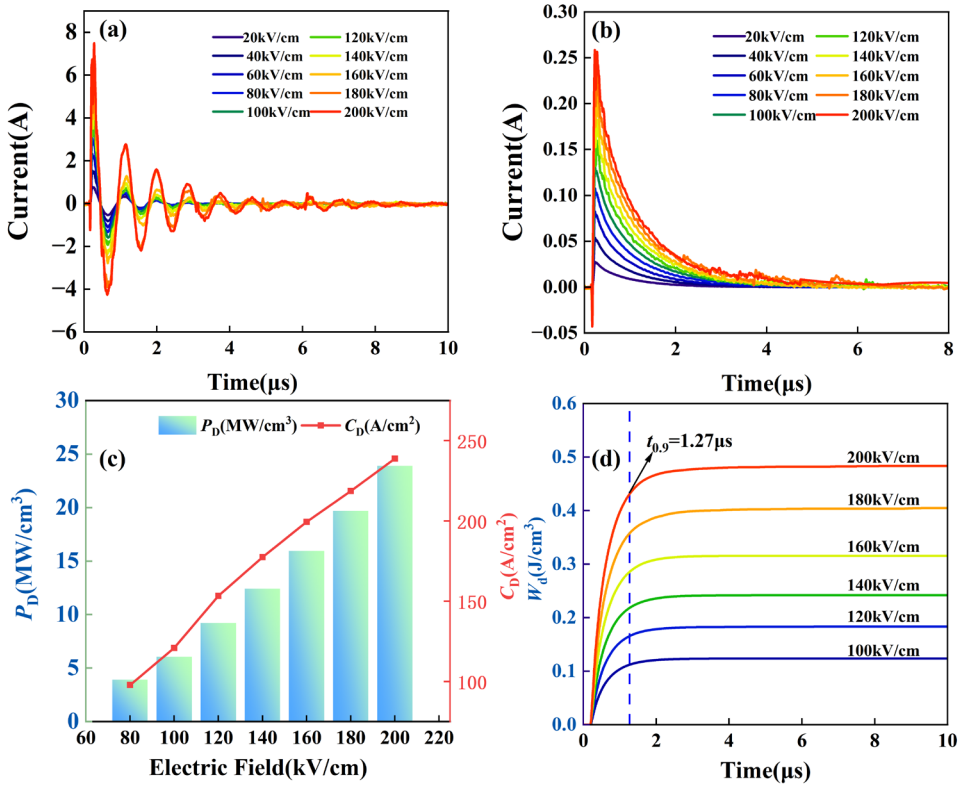

Figure 5. a) Plots of underdamped charge/discharge profiles of (1-*x*)KNN-*x*KBZN ceramics; (b)current density and power density of (1-*x*)KNN-*x*KBZN ceramics; (c) overdamped charge/discharge profiles of (1-*x*)KNN-*x*KBZN ceramics; (d) discharge energy density and time of discharge of (1-*x*)KNN-*x*KBZN ceramics.

 doi:10.20944/preprints202509.1110.v1

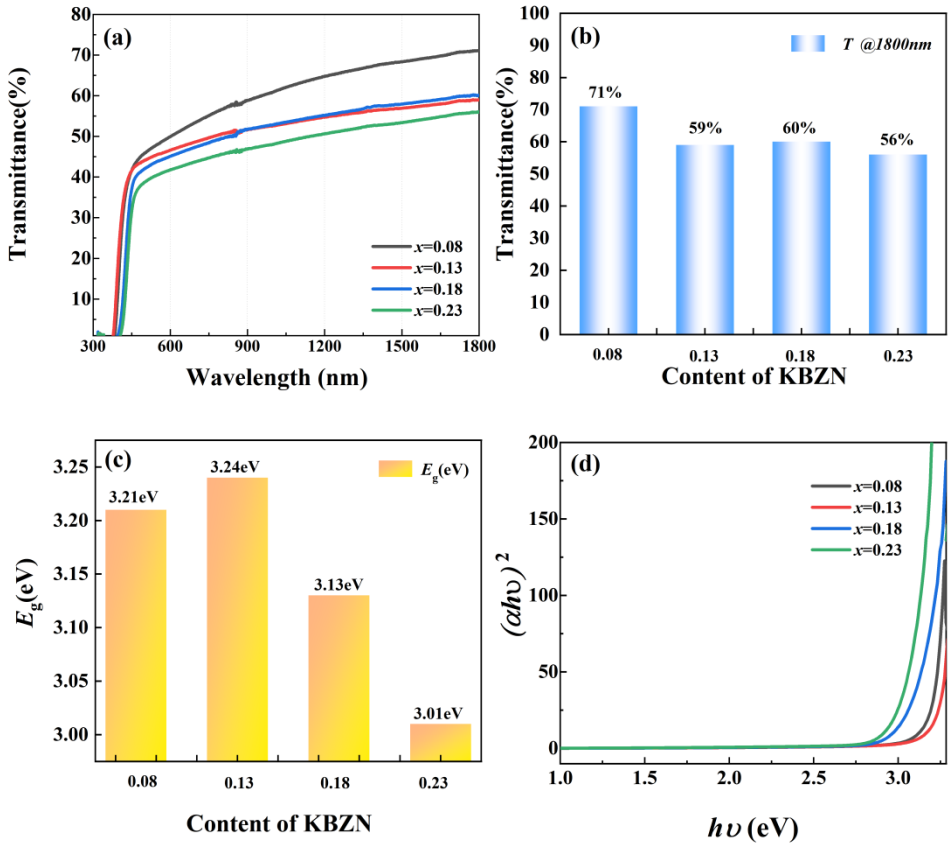

Figure 6. (a-b) Optical transmittance diagrams of (1-x)KNN-xKBZN ceramics; (c-d) Optical band gap diagrams of (1-x)KNN-xKBZN ceramics.

Optical energy loss in ceramics primarily occurs through photoelectron transitions between the conduction and valence bands. A proven strategy to minimize such losses involves widening the bandgap, which reduces electron delocalization effects. Under low-intensity illumination, the increased bandgap suppresses electron excitation, thereby enhancing material transparency. The optical bandgap (E_g) can be quantitatively determined using the Tauc equation:

$$(\alpha h\nu)^2 = A(h\nu - E_g) \quad (5)$$

$$\alpha = -\ln T / t \quad (6)$$

$$\nu = \frac{c}{\lambda} \quad (7)$$

where h represents Planck's constant, A is a constant, α is the absorption rate, ν is the photon frequency, T is the transmittance, and t is the sample thickness.

Figure 6(a) displays the linear transmittance spectra of 0.3 mm-thick (1-x)KNN-xKBZN ceramics across the 250-1800 nm wavelength range. The transmittance exhibits a rapid initial rise with increasing wavelength, followed by a plateau region at longer wavelengths. Quantitative analysis (Figure 6(b)) reveals that the optical transmittance systematically decreases from 71% to 56% with increasing KBZN content. Bandgap analysis was performed by fitting the transmittance data from Figure 6(a) using the Tauc method (Figure 6(d)), demonstrating that KBZN incorporation increases the optical bandgap (E_g) by more than 3 eV in all compositions. As shown in Figure 6(c), the bandgap displays a non-monotonic dependence on KBZN content, initially increasing before decreasing at higher doping levels. This bandgap widening effect directly correlates with enhanced optical transmittance, explaining the exceptional transparency achieved in the (1-x)KNN-xKBZN ceramic[42-44].

 doi:10.20944/preprints202509.1110.v1

4. Conclusions

In this study, (1-x)KNN-xKBZN transparent ferroelectric ceramics were successfully prepared by a solid-state method. The results demonstrate that KBZN incorporation effectively modifies the ceramic phase structure and enhances grain uniformity, consequently improving the breakdown field strength. 0.87KNN-0.13KBZN composition exhibited superior energy storage performance, achieving a total energy storage density (W = 3.18 J/cm³), recoverable energy density ((W_{rec} = 2.51 J/cm³), and efficiency (η = 79%) at 220 kV/cm. Pulsed charge/discharge measurements revealed outstanding current density (C_D = 248.73 A/cm²), power density (P_D = 23.88 MW/cm³), and ultrafast discharge characteristics ($t_{0.9}$ = 1.27 μs) at 200 kV/cm. Furthermore, KBZN doping-induced bandgap engineering significantly widened the optical bandgap (> 3 eV), directly resulting in enhanced transmittance (T = 71% at 1800 nm). These findings confirm that the (1-x)KNN-xKBZN system successfully resolves the critical challenge of balancing optical transparency with ferroelectric properties in KNN-based ceramics, providing promising avenues for future research in transparent ferroelectric materials.

Funding: This work was supported by Xi'an Science and Technology Project [No. 2024JH-GXFW-0082]; and the Foreign Experts Program of Science and Technology Ministry [No. G2023041034L; No. G2023041001L].

Data Availability Statement: The data that support the findings of this study are available from the corresponding author upon reasonable request.

Acknowledgments: This work was supported by Xi'an Science and Technology Project (No. 2024JH-GXFW-0082) and the Foreign Experts Program of Science and Technology Ministry (No. G2023041034L; No. G2023041001L).

Conflicts of interest: The authors declare that they have no known competing financial interests or personal relationships that could have appeared to influence the work reported in this paper.

References

1. Guo M, Jiang J, Shen Z, et al. High-energy-density ferroelectric polymer nanocomposites for capacitive energy storage: enhanced breakdown strength and improved discharge efficiency. Materials Today, 2019, 29: 49-67.
2. Zhao P, Cai Z, Chen L, et al. Ultra-high energy storage performance in lead-free multilayer ceramic capacitors via a multiscale optimization strategy. Energy & Environmental Science, 2020, 13(12): 4882-4890.
3. Yang L, Kong X, Li F, et al. Perovskite lead-free dielectrics for energy storage applications. Progress in Materials Science, 2019, 102: 72-108.
4. Xing J, Li X, Xu D, et al. Intrinsic and extrinsic contributions to energy storage performance in potassium sodium niobate-based ceramics. Journal of the American Ceramic Society, 2024, 107(7): 4824-4835.
5. Yang L, Kong X, Li Q, et al. Excellent energy storage properties achieved in sodium niobate-based relaxor ceramics through doping tantalum. ACS Applied Materials & Interfaces, 2022, 14(28): 32218-32226.
6. Zheng L, Sun P, Zheng P, et al. Significantly tailored energy-storage performances in $Bi_{0.5}Na_{0.5}TiO_3$-$SrTiO_3$-based relaxor ferroelectric ceramics by introducing bismuth layer-structured relaxor $BaBi_2Nb_2O_9$ for capacitor application. Journal of Materials Chemistry C, 2021, 9(15): 5234-5243.
7. Wu S, Fu B, Zhang J, et al. Superb energy storage capability for $NaNbO_3$-based ceramics featuring labyrinthine submicro-domains with clustered lattice distortions. Small, 2023, 19(45): 2303915.
8. Zhang M, Yang H, Lin Y, et al. Significant increase in comprehensive energy storage performance of potassium sodium niobate-based ceramics via synergistic optimization strategy. Energy Storage Materials, 2022, 45: 861-868.
9. Liu C, Dai Z, Zheng Y, et al. Preparation and investigation of $K_{0.5}Na_{0.5}NbO_3$-$Bi(Sr_{0.5}Hf_{0.5})O_3$ transparent energy storage ceramic. Journal of Power Sources, 2025, 640: 236759.

 doi:10.20944/preprints202509.1110.v1

10. Yang Z, Gao F, Du H, et al. Grain size engineered lead-free ceramics with both large energy storage density and ultrahigh mechanical properties. Nano Energy, 2019, 58: 768-777.
11. Xing J, Huang Y, Wu B, et al. Energy storage behavior in $ErBiO_3$-doped (K, Na) NbO_3 lead-free piezoelectric ceramics. ACS Applied Electronic Materials, 2020, 2(11): 3717-3727.
12. Zou K, Dan Y, Xu H, et al. Recent advances in lead-free dielectric materials for energy storage. Materials Research Bulletin, 2019, 113: 190-201.
13. Wu J. Advances in lead-free piezoelectric materials. Singapore: Springer, 2018.
14. Lang R, Chen Q, Gao T, et al. $BaTiO_3$-based lead-free relaxor ferroelectric ceramics for high energy storage. Journal of the European Ceramic Society, 2024, 44(6): 3916-3925.
15. Zhao X, Chao X, Wu D, et al. Evaluation of birefringence contribution to transparency in (1-x)KNN-xSr($Al_{0.5}Ta_{0.5}$)O_3 ceramics: a phase structure tailoring. Journal of Alloys and Compounds, 2019, 798: 669-677.
16. Xing J, Huang Y, Wu B, et al. Energy storage behavior in $ErBiO_3$-doped (K, Na) NbO_3 lead-free piezoelectric ceramics. ACS Applied Electronic Materials, 2020, 2(11): 3717-3727.
17. Zhang L, He M, Shao S. Machine learning for halide perovskite materials. Nano Energy, 2020, 78: 105380.
18. Deng D, Irshad M S, Kong X, et al. Potassium sodium niobate-based transparent ceramics with high piezoelectricity and enhanced energy storage density. Journal of Alloys and Compounds, 2023, 953: 170081.
19. Qiao L, Li G, Tao H, et al. Full characterization for material constants of a promising KNN-based lead-free piezoelectric ceramic. Ceramics International, 2020, 46(5): 5641-5644.
20. Dai Z, Li D, Zhou Z, et al. A strategy for high performance of energy storage and transparency in KNN-based ferroelectric ceramics. Chemical Engineering Journal, 2022, 427: 131959.
21. Wang J, Li Y, Sun N, et al. Bi($Mg_{0.5}Ti_{0.5}$)O_3 addition induced high recoverable energy-storage density and excellent electrical properties in lead-free $Na_{0.5}Bi_{0.5}TiO_3$-based thick films. Journal of the European Ceramic Society, 2019, 39(2-3): 255-263.
22. Yan F, Huang K, Jiang T, et al. Significantly enhanced energy storage density and efficiency of BNT-based perovskite ceramics via A-site defect engineering. Energy Storage Materials, 2020, 30: 392-400.
23. Dai Z, Wang S, Liu Y, et al. Energy storage performance of $SrSc_{0.5}Nb_{0.5}O_3$ modified (Bi,Na)TiO_3-based ceramic under low electric fields. Journal of the American Ceramic Society, 2023, 106(4): 2366-2374.
24. Zhang Y, Zuo R. Excellent energy-storage performances in La_2O_3 doped (Na, K) NbO_3-based lead-free relaxor ferroelectrics. Journal of the European Ceramic Society, 2020, 40(15): 5466-5474.
25. Dai Z, Xie J, Chen Z, et al. Improved energy storage density and efficiency of (1-x)$Ba_{0.85}Ca_{0.15}Zr_{0.1}Ti_{0.9}O_3$-$x$$BiMg_{2/3}Nb_{1/3}O_3$ lead-free ceramics. Chemical Engineering Journal, 2021, 410: 128341.
26. Zhang Y, Lin Y, Ma Y, et al. Synergistically enhanced discharged energy density and efficiency achieved in designed polyetherimide-based composites via asymmetrical interlayer structure induced optimized interface effectiveness. Materials Horizons, 2024, 11(19): 4759-4768.
27. Chai Q, Yang D, Zhao X, et al. Lead-free (K, Na) NbO_3-based ceramics with high optical transparency and large energy storage ability. Journal of the American Ceramic Society, 2018, 101(6): 2321-2329.
28. Liu T, Chen Y, Zheng Z, et al. The high nano-domain improves the piezoelectric properties of KNN lead-free piezo-ceramics. Ceramics International, 2023, 49(15): 25035-25042.
29. Lin J, Ge G, Zhu K, et al. Simultaneously achieving high performance of energy storage and transparency via A-site non-stoichiometric defect engineering in KNN-based ceramics. Chemical Engineering Journal, 2022, 444: 136538.
30. Yang Z, Du H, Jin L, et al. High-performance lead-free bulk ceramics for electrical energy storage applications: design strategies and challenges. Journal of Materials Chemistry A, 2021, 9(34): 18026-18085.
31. Dai Z, Xie J, Liu W, et al. Effective strategy to achieve excellent energy storage properties in lead-free

 doi:10.20944/preprints202509.1110.v1

$BaTiO_3$-based bulk ceramics. ACS Applied Materials & Interfaces, 2020, 12(27): 30289-30296.

32. Dai Z, Xie J, Fan X, et al. Enhanced energy storage properties and stability of $Sr(Sc_{0.5}Nb_{0.5})O_3$ modified $0.65BaTiO_3$-$0.35Bi_{0.5}Na_{0.5}TiO_3$ ceramics. Chemical Engineering Journal, 2020, 397: 125520.
33. Dang Z, Lin Y, Yuan Q, et al. Ultrahigh Dielectric Energy Density and Efficiency in PEI-Based Gradient Layered Polymer Nanocomposite. Advanced Functional Materials, 2024, 34(41): 2406148.
34. Shi C, Ma J, Wu J, et al. Coexistence of excellent piezoelectric performance and high Curie temperature in KNN-based lead-free piezoelectric ceramics. Journal of Alloys and Compounds, 2020, 846: 156245.
35. Rubio-Marcos F, Fernandez J F, Ochoa D A, et al. Understanding the piezoelectric properties in potassium-sodium niobate-based lead-free piezoceramics: Interrelationship between intrinsic and extrinsic factors. Journal of the European Ceramic Society, 2017, 37(11): 3501-3509.
36. Hu R, Lin Y, Zhang M, et al. Enhancement of recoverable energy density and efficiency of $K_{0.5}Na_{0.5}NbO_3$ ceramic modified by $Bi(Mg_{0.5}Zr_{0.5})O_3$. Materials Today Energy, 2022, 30: 101185.
37. Li Z, Zhang B, Zhang Z, et al. Vitamin needed: Lanthanides in optoelectronic applications of metal halide perovskites. Materials Science and Engineering: R: Reports, 2023, 152: 100710.
38. Hou J, Dai Z, Liu C, et al. Enhanced photoelectric properties for $BiZn_{0.5}Zr_{0.5}O_3$ modified KNN-based lead-free ceramics. Journal of Alloys and Compounds, 2023, 960: 170639.
39. Zhu H, Zhang X, Zhang M, et al. Structure and electrical properties of $SrZrO_3$-modified (K, Na, Li)(Nb, Ta) O_3 lead-free piezoelectric ceramics. Journal of Materials Science: Materials in Electronics, 2018, 29: 3905-3911.
40. Gupta A, Kumar R, Singh S. Coexistence of negative and positive electrocaloric effect in lead-free $0.9(K_{0.5}Na_{0.5})NbO_3$-$0.1SrTiO_3$ nanocrystalline ceramics. Scripta Materialia, 2018, 143: 5-9.
41. Wang J, Li Y, Sun N, et al. $Bi(Mg_{0.5}Ti_{0.5})O_3$ addition induced high recoverable energy-storage density and excellent electrical properties in lead-free $Na_{0.5}Bi_{0.5}TiO_3$-based thick films. Journal of the European Ceramic Society, 2019, 39(2-3): 255-263.
42. Ma W, Zhu Y, Marwat M A, et al. Enhanced energy-storage performance with excellent stability under low electric fields in BNT-ST relaxor ferroelectric ceramics. Journal of Materials Chemistry C, 2019, 7(2): 281-288.
43. Gan X, Yang H, Lin Y, et al. Improving the energy storage performances of $Bi(Ni_{0.5}Ti_{0.5})O_3$-added $K_{0.5}Na_{0.5}NbO_3$-based ceramics. Ceramics International, 2022, 48(10): 14920-14927.
44. Zhang M, Yang H, Yu Y, et al. Energy storage performance of $K_{0.5}Na_{0.5}NbO_3$-based ceramics modified by $Bi(Zn_{2/3}(Nb_{0.85}Ta_{0.15})_{1/3})O_3$. Chemical Engineering Journal, 2021, 425: 131465.